Science of the Total Environment 725 (2020) 138258

Contents lists available at ScienceDirect

Science of the Total Environment

journal homepage: www.elsevier.com/locate/scitotenv

Oxygenation and synchronous control of nitrogen and phosphorus release at the sediment-water interface using oxygen nano-bubble modified material

Jingfu Wang [a,*], Jingan Chen [a,*], Pingping Yu [a,b], Xiaohong Yang [a,b], Lijuan Zhang [c,d], Zhanli Geng [d], Kangkang He [a,b]

[a] State Key Laboratory of Environmental Geochemistry, Institute of Geochemistry, Chinese Academy of Sciences, Guiyang 550002, PR China
[b] College of Resource and Environmental Engineering, Guizhou University, Guiyang 550025, PR China
[c] Shanghai Synchrotron Radiation Facility, Shanghai Advanced Research Institute, Chinese Academy of Sciences, Shanghai 201204, PR China
[d] Shanghai Institute of Applied Physics, Chinese Academy of Sciences, Shanghai 201800, PR China

HIGHLIGHTS

- Oxygen nano-bubble modified mineral (ONBMM) was developed.
- ONBMM effectively improved DO levels near the sediment-water interface.
- Fluxes of TP, NH_3-N, and TN loading from sediment reduced by 96%, 51%, and 25%.
- ONBMM has great application potential in internal pollution control in lakes.

GRAPHICAL ABSTRACT

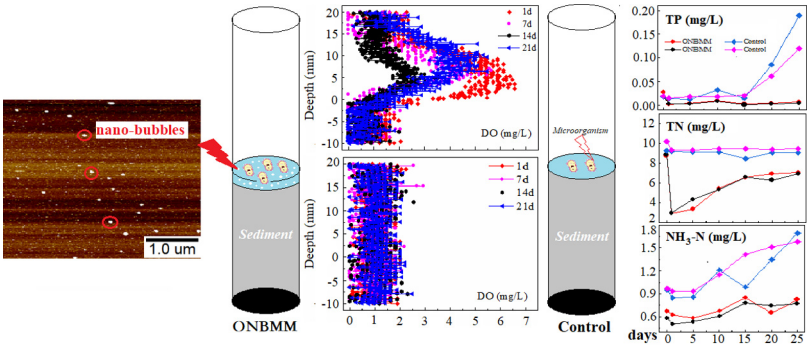

ARTICLE INFO

Article history:
Received 3 February 2020
Received in revised form 11 March 2020
Accepted 26 March 2020
Available online 27 March 2020

Editor: Dr. Ouyang Wei

Keywords:
Oxygen nano-bubble
Phosphorus
Nitrogen
Sediment-water interface
Eutrophication

ABSTRACT

Synchronously controlling the nitrogen (N) and phosphorus (P) release from sediments is an important basis for eutrophication management in lakes, but it is still a technical challenge at present. Loading nano-bubbles on the surface of natural minerals to increase dissolved oxygen(DO) level at the sediment-water interface (SWI)provides a possible solution to this problem. In this study, oxygen nano-bubble modified mineral (ONBMM) technology was developed, and its efficiency of oxygenation at the SWI and effect on the removal of internal nutrient input were evaluated under simulated conditions. The results showed that ONBMM effectively improved DO levels near the SWI; the highest concentration reached 6.55 mgL^{-1}. Meanwhile, adding ONBMM remarkably reduced the concentrations of total P(TP), total N(TN) and ammonia N(NH_3-N) in the overlying water. Compared with the control group, the fluxes of TP, NH_3-N, and TN loading from sediments in simulation cores treated with ONBMM reduced by 96.4%, 51.1%, and 24.9%, respectively. The high-resolution data obtained by DGT showed that ONBMM effectively inhibited the reduction and release of Fe—P through increasing the oxygen level at the SWI. The results of 16S rRNA high-throughput sequencing showed that adding ONBMM strengthened the

* Corresponding authors.
E-mail addresses: wangjingfu@vip.skleg.cn (J. Wang), chenjingan@vip.skleg.cn (J. Chen).

https://doi.org/10.1016/j.scitotenv.2020.138258

role of nitrobacteria, denitrifying bacteria, and ammonia oxidation bacteria at the SWI. The ONBMM technology provides a new tool to achieve oxygenation at the SWI and *in situ* control of internal pollution in eutrophic lakes.

1. Introduction

Excess input of nitrogen (N) and phosphorus (P) is an important factor causing water eutrophication in lakes and reservoirs (Smith and Schindler, 2009). Limiting nutrient sources is one way to restore eutrophic water bodies (Smith, 2003). The source of N and P in lakes is mainly divided into external pollution (domestic sewage, industrial wastewater, agricultural surface source pollution, *etc.*) and internal pollution (nutrients release from sediment). When external inputs are effectively controlled, the deposited P, N, and other nutrients can migrate and be released to the sediment-water interface (SWI) due to seasonal variations of water temperature and dissolved oxygen (DO) concentration or strong biological effects (Wang et al., 2015, 2016). This provides a steady stream of supply to the water. Therefore, effectively controlling the release of internal pollutants is important for restoring eutrophic lakes.

Previous studies found that the oxygen state at the SWI was strongly correlated with the N and P transport and release rate (Beutel et al., 2008; Ding et al., 2016). The aerobic conditions could inhibit the release of nutrients from sediments to overlying water (Nausch et al., 2009; Wang et al., 2016). Improving the DO concentrations at the SWI is one important way to control the release of sedimentary nutrients in the lake.

Research on the theory and technology of oxygenation in lakes began in the 1940s. Originally, Mercier and Perret (1949) developed the earliest deep-water oxygenation system. Currently widely-used deep-water oxygenation technologies include Speece conical technology, bubble plume diffusion technology (McGinnis et al., 2004), artificial de-layer technology (Serra et al., 2007) and gas lift technology (Ashley et al., 2008). However, these technologies focus on increasing DO level at the bottom of the lake (or reservoir) and are not oriented toward to the SWI oxygenation. Therefore, these technologies, which require complex hardware and high operational costs, are limited in controlling the release of internal pollutants in lakes.

Since the 21st century, the emergence of gaseous nano-technology has enabled research on oxygenation techniques at the SWI in lakes (Zhang et al., 2018). The concept of the nano-bubble (NB) was first introduced by Parker et al. (1994) when researching the hydrophobic long-range self-gravity of two solid surfaces. An atomic force microscope (AFM) image of NB was first published in 2000 (Ishida et al., 2000). Several experimental validations showed that nano-bubbles did exist in the solid-liquid interface. Subsequent studies found that NB could stably exist in multiple solid-liquid interfaces for hours up to days (Ducker, 2009; Seddon et al., 2011). NB is characterized by surface with charge (Ushikubo et al., 2010), gas-liquid interface with strong hydrogen bond (Agarwal et al., 2011), high internal density (Zhang et al., 2008), *etc.*, which is an important reason for the long-term stability of NB. In addition, the specific surface area of NB is distinctly larger compared to the bubbles at macro and millimeter scales produced by traditional aeration. As such, NB has an extremely high mass transfer efficiency of oxygen.

With its high stability and high oxygen-transfer efficiency (Tyrrell and Attard, 2001; Fang et al., 2018), NB has significant potential to be applied in the oxygenation and *in situ* control of internal-nutrient release at the SWI in lakes (Zhang et al., 2018; Yu et al., 2019). In this study, oxygen NB modified mineral (ONBMM) was developed and applied to conduct an experimental study on the oxygen enrichment and *in situ* control of N and P pollutants at the SWI. High-resolution planar luminescent optode (PO) technology was used to detect the profile distribution of DO concentration at the SWI. The concentrations of total P (TP), total N (TN), ammonia N (NH_3-N) in the overlying water were measured to quantify the temporal variation in each nutrient's release flux at the SWI. Meanwhile, the microbial community composition of surface sediments was analyzed using 16S rRNA amplicon sequencing techniques. The objectives of this study were: 1) to test the efficiency of ONBMM on oxygenation and the synchronization control of N and P release at the SWI; 2) to reveal the mechanism involved in the ONBMM control of internal-nutrient loading; and 3) to provide a new technology for efficient oxygenation and *in situ* control of sediment pollution at the SWI in eutrophic lakes.

2. Materials and methods

2.1. Sampling and experimental simulation

Four parallel sediment-core samples were collected using a gravity sampler in Hongfeng Reservoir, a large deep-water eutrophic reservoir in southwest China. It is a seasonally anoxic water body. The DO concentration in the bottom water is <1 mgL^{-1} from late spring to early autumn. In the surface 5 cm of sediment, the TP content ranged from 766 to 4306 mg kg^{-1} (mean: 1815 mg kg^{-1}, $n = 108$). The TN content ranged from 0.27% to 0.78% (mean: 0.38%), and the total organic carbon (TOC) content varied from 1.99% to 10.62% (mean: 3.97%) (Wang et al., 2016, Wang et al., 2017a, b). After collection, each column core was sealed with a rubber stopper and wrapped in tin foil to avoid light. The cores were then quickly brought back to the laboratory. The inner diameter of the column core was 11 cm and the length was 100 cm. In the sediment-core samples, the height ratio of sediment to water was approximately 1: 4. In the field, 20 L bottom water samples were collected using a Niskin sampler to support simulation experiments.

The experimental settings of samples treated and untreated with ONBMM were compared, with two parallels for each group. The overlying water was controlled in an anaerobic state (DO<1 mgL^{-1}) by continuously feeding a sufficient amount of high purity N_2 into the column core. During the experiment, the simulation device remained under dark conditions. The temperature of the column core was controlled at 20 °C ± 1 °C. The simulated environmental conditions were consistent with the bottom water conditions in Hongfeng Reservoir in summer. The period of simulation experiment was 25 days. The overlying water samples were collected on Days 0, 5, 10, 15, 20, and 25. After each sampling event, the same volume of bottom water was added to each sample. These volumes were calibrated in subsequent calculations. The prepared ONBMM was respectively added to the sediment-core to make it settle at the SWI. On days 0and 5, the ZrO-Chelex DGT (Easysensor Ltd., Nanjing, China) was plugged at the SWI of the column core and recycled after standing for 24 h.

2.2. Preparation of ONBMM and characterization of surface Nanobubbles

In this study, NBs were prepared using the alcohol-water substitution method. 1) Pure oxygen was injected into ethanol (300 mL min^{-1}, purity >99%), and saturated ethanol solution was obtained at 20 °C for 30 min. 2) Add 100 g Muscovite mineral particles. 3) After standing for 10 min, ethanol was replaced by pure water (V_1:V_2 = 9:1, where V_1 denotes the volume of ultrapure water and V_2 denotes the volume of methanol). Finally, NBs formed on the mineral surface, due to oversaturation. Detailed operational steps were described in Yu et al. (2019).

NBs on the ONBMM surface were characterized using atomic force microscopy (AFM). AFM measurements were performed using a Bruker Multimode 8 SPM with NanoScope 8 software and one NanoScope V controller. Images of the NBs on the mica surfaces were observed using atomic force microscopy (TM-AFM), with a silicon nitride cantilever beam with a spring constant of 0.35 N m (DNP-10, Bruker). In the tapping mode, peak force amplitude, peak force frequency, and scanning rate were set as 100 nm, 2 kHz and 0.977 Hz, respectively. The loading force was set from 100 PN to 400 PN. The AFM test of sample was completed ata room temperature of 25 °C. Finally, Bruker's nanoscope analysis software was used to process the AFM image. The test above was completed in the AFM laboratory of Shanghai Institute of Applied Physics, Chinese Academy of Sciences.

2.3. Composition analysis of hydrochemistry and microbial communities

The TP concentration in overlying water was measured using the molybdenum-blue method (Murphy and Riley, 1962). TN concentration was determined using alkaline potassium persulfate-hydronaphthalene ethylenediamine spectrophotometry (Yue et al., 2014). After being filtered through a 0.45 μm glass fiber microfiltration membrane, NH_3-N levels were determined by using Nessler's reagent spectrophotometry. DO distribution near the SWI was determined using PO (VisiSense TD, PreSens Precision Sensing GmbH, Germany). Prior to the addition of ONBMM, plane electrode films were cut into a long strip, with a size of 1 cm × 10 cm; these were previously adhered to the inner wall of the upper part in the sampling tube. Meanwhile, the temporal variations in the DO in the overlying water was measured using multi-parameter water quality monitors (YSI6600V2, YSI Inc., Yellow Springs, USA). DGT probes were retrieved 24 h after insertion and cleaned with deionized water. The ZrO-Chelex gels were then cut with an interval of 2 mm and placed into 1.5 mL centrifuge tubes. The DGT-Fe and DGT-P were extracted using 1 mol/L nitric acid and 1 mol/L sodium hydroxide solution, respectively, and measured by the phenanthroline colorimetric method (Tamura et al., 1974; Ding et al., 2016) and the molybdenum blue method (Murphy and Riley, 1962), respectively.

Fresh sediment samples were collected at a depth of 0–2 cm below the surface (mass ≥ 5 g, at least 3 points were mixed for each sample) and were placed in a sterile centrifuge tube. The structure and diversity of the microbial communities were characterized using DNA extraction, PCR amplification, and 16S sequencing. The genomic DNA was extracted from the sample using the CTAB method. After that, the DNA purity and concentration levels were detected using agarose gel electrophoresis. A proper amount of sample DNA was collected in the centrifuge tube and diluted to 1 ngμL^{-1} with sterile water. The diluted genomic DNA was used as a template. Based on the selection in the sequencing region, the PCR was conducted using the Phusion® High-Fidelity PCR Master Mix with GC Buffer and high-efficiency high-fidelity enzymes from New England Biolabs. The efficiency and accuracy of amplification was controlled using specific primers with Barcode. The PCR product was detected using agarose gel electrophoresis with a 2% concentration. Fifteen samples were sequenced using the Ion S5 platform and Clean reads were produced. The tests were completed at the Beijing Nohezhiyuan Biological Information Technology Co., Ltd. in China.

2.4. Release flux of nutrients in SWI

Changes in thenutrient concentrations in the overlying water over time were used to calculate the input flux of nutrients at the SWI. The average nutrient release flux (R) was calculated according to the mass balance eq. (1):

$$R = \left[V(C_n - C_0) + \sum_{j=1}^{n} V_{j-1}(C_{j-1} - C_a) \right] / (A \times t) \quad (1) \qquad (1)$$

In this expression, R, V, C_0, C_n, C_{j-1}, C_a, V_{j-1}, A, and t denote the release rate [mgm^{-2}d^{-1}]; volume of overlying water (L); concentration of nutrient substances in overlying water in the first, second and j-1 sampling (mgL^{-1}); nutrient concentration of the added water (mgL^{-1}); the first sampling volume (L); the water-sediment contact interface (m^2) in the sediment column sample; and release time (d), respectively.

2.5. Analysis of community structure diversity

To study the species composition of each sample, Clean reads of 15 samples were clustered using the Uparse (Uparse v7.01001) software. The sequence was clustered into OTUs (Operational Taxonomy Units) at a 97% similarity level. The species were then annotated and analyzed using the SSU rRNA database of Mothur method and SILVA132with a 0.8 to 1 threshold value. Taxonomic information was collected and community compositions of each sample were statistically identified at all taxonomic levels: kingdom, phylum, class, order, family, genus, and species.

Based on the species abundance of samples in the OTU list, Qiime software version 1.9.1 was used to calculate the abundance index, Chao index, ACE index, community Shannon index, and Simpson index. Three parallel sample data in the group were imported into the Qiime software in batches to analyze the intergroup difference of the OTU table. The distribution graphs of species abundance tables and multi-sample species were generated at different taxonomic levels.

2.6. Statistical analysis

Origin 2017 (Origin Lab Inc., USA), SigmaPolt 14.0 (Systat Software Inc., USA) and R software (Version 2.15.3) were used to generate drawings. The statistical software package SPSS 23.0 (IBM Corp., USA) was used for data analysis. Uparse software (Uparse v7.0.1001) was used to conduct the cluster analysis of the Clean Reads. Qiime software (Version 1.9.1) was used to calculate the diversity index.

3. Results and discussion

3.1. AFM image of nano-bubbles on ONBMM surface

AFM scanning was carried out on the white mica substrate and the developed ONBMM. Fig.1a-b shows the height and phase image of 6000 mesh mica particles (the untreated raw minerals) under AFM. The mica sheet was characterized by a layered distribution, with a granular, irregular, and uneven appearance. After processing, many white dots were generated on the ONBMM surface. The stiffness values of these white dots changed from 0.08 Nm^{-1} to 0.2 Nm^{-1}. This is consistent with the range of NB stiffness (0.06–0.2 Nm^{-1}) (Wang et al., 2017a, b). Fig. 1c-d shows that the stiffness levels of the most white dots lay within the bubble stiffness. Some mineral surface loaded little oxygen NBs (Fig. 1c-d), which were difficult to characterize using AFM. Overall, NBs on the surface of ONBMM could be clearly observed. The newly developed materials were confirmed as the gaseous science and technology materials at the nano-level. This also provides strong evidence for the increase of DO in SWI.

3.2. Effect of ONBMM on DO distribution at SWI

After the addition of ONBMM, the DO in SWI experienced a peak in concentration (Fig. 2). After one day, there was one obvious DO peak (Fig. 2A-B) in the range of 0–10 mm near the SWI of two parallel column cores. The highest DO concentrations in column core A and column core B reached 6.55 mgL^{-1} and 5.96 mgL^{-1}, respectively. In the samples without added ONBMM, there was no DO concentration peak near the SWI of the two parallel column cores, indicating that there was no aerobic zone generated near the SWI (Fig.2C-D). On Days 7, 14, and 21, in the column core samples treated with ONBMM, the DO concentration

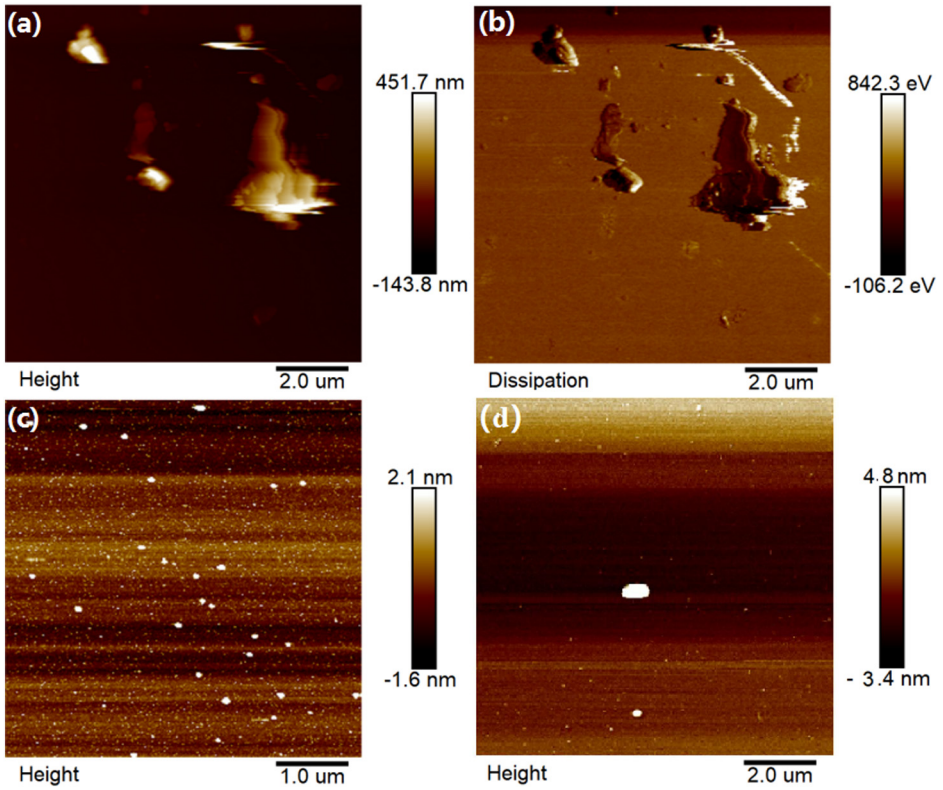

Fig. 1. AFM images of white mica substrate and nano-bubbles. (a) AFM height image and (b) phase image of 6000 mesh mica particle raw mineral in air, (c) AFM image of nano-bubbles on mica sheet after alcohol-water replacement, (d) AFM graph of mica partical alcohol-water replacement.

remained high in the 20 mm range near the SWI. The highest concentration in column core B reached 6.38 mgL^{-1} on Day 21. It was difficult to precisely control the oxygen loading of the ONBMM during the experiment, leading the fluctuations of DO level in different periods. But the observational data shown that the parallel cores treated with ONBMM both obtained high DO level at the SWI. The ONBMM

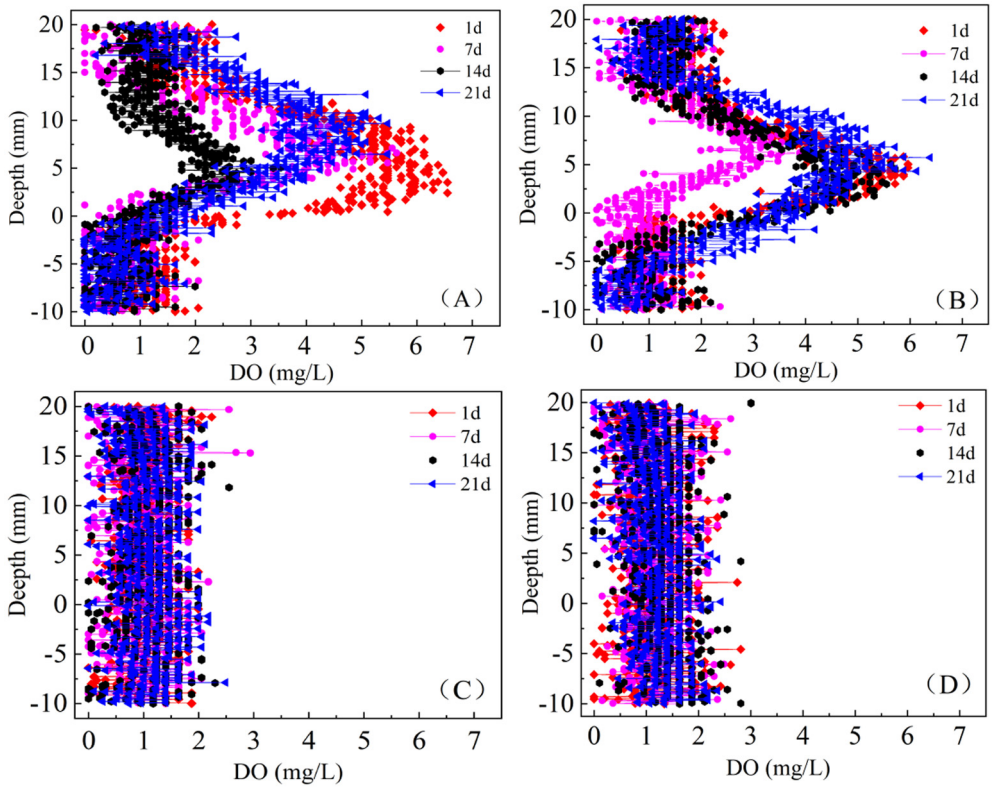

Fig. 2. Changes in the DO concentration at the SWI in the samples treated with ONBMM (A, B) and untreated with ONBMM group (C, D).

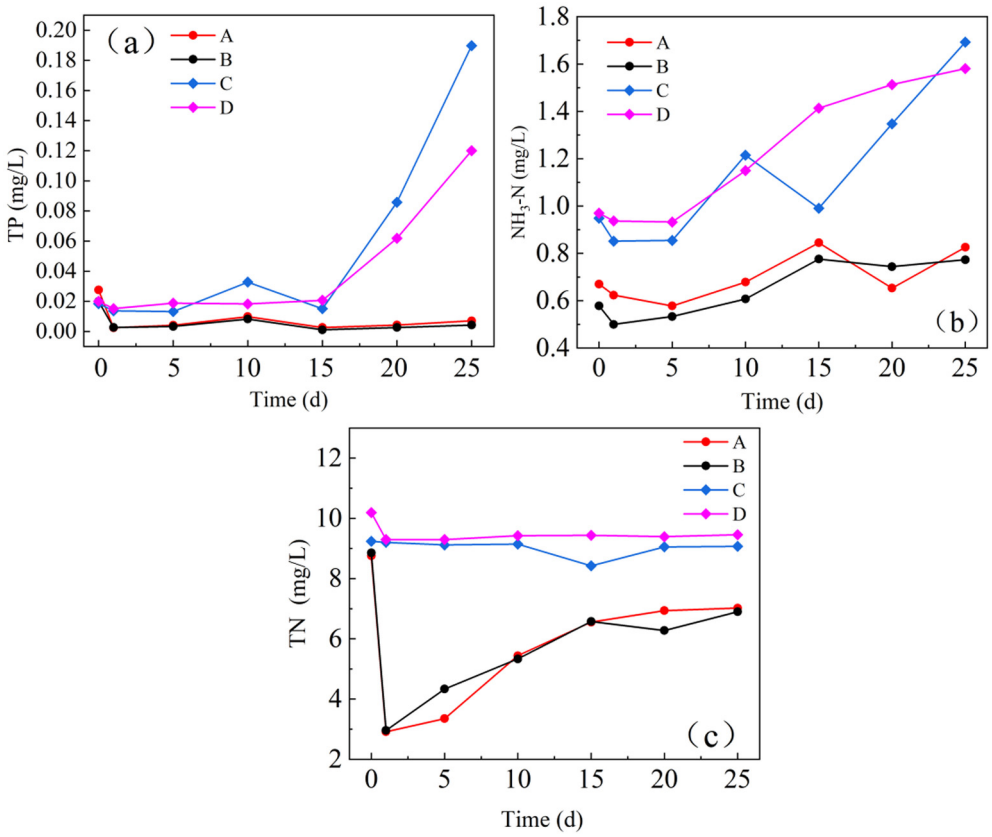

Fig. 3. Changes in the TP, NH_3-N, and TN concentrations in overlying water of the sediment column cores when treated with ONBMM (A,B) and when untreated with ONBMM (C,D).

treatment obviously increased the DO concentration at the SWI in the column cores.

3.3. Mechanism of ONBMM inhibiting the release of P from sediments

In the group untreated with ONBMM, the average TP concentrations in the overlying water (Fig. 3a) continued to increase from 0.01 mgL^{-1} to 0.15 mgL^{-1}. The average TP concentrations in the group treated with ONBMM in the overlying water were apparently lower compared to the group untreated with ONBMM. The average TP concentration in the overlying water was distinctly reduced, from 0.02 mgL^{-1} to 0.002 mgL^{-1}. The TP removal rate reached 96.4%. Bioavailability is an important index to evaluate the environmental risk of P. Generally, dissolved inorganic P is considered to be the most easily utilized form by algae. Most of the P release from sediment, under conditions without disturbance, is dissolved inorganic P (Wang et al., 2016).

Because the group treated with ONBMM has always maintained a high level of DO (>2 mgL^{-1}), which has achieved the purpose of inhibiting the release of P under the condition of full oxygen (Fig. 3). In two cores with ONBMM, the release fluxes of TP from sediment were −0.72 and −0.60 $mgm^{-2}d^{-1}$ (with the mean value of −0.66 $mgm^{-2}d^{-1}$) (Table 1). In two cores that were untreated with ONBMM, the release fluxes of sediment TP were 5.58 and 3.39 $mgm^{-2}d^{-1}$ (with the mean value of 4.49 $mgm^{-2}d^{-1}$). There were significant differences in TP concentration and SWI release fluxes in the overlying water when comparing the samples treated and untreated with ONBMM (Fig. 3a and Table 1). These results showed that the ONBMM strongly inhibited the release of P from sediment.

In the group untreated with ONBMM, P was released from the sediment to the overlying water. When ONBMM was added, the P was effectively inhibited with respect to variations in concentrations and the release fluxes of TP into the overlying water. Fig. 4 showed that the concentrations of DGT-Fe and DGT-P decreased to nearly 0 in the depths of 0–10 mm in the cores after 5 days treated with ONBMM, while in the control groups, their concentrations did not significantly decrease near SWI. The sediment P in Hongfeng included mainly Fe-bound P (Fe-P) (Wang et al., 2016). The reduction and dissolution of Fe-P dominated the P release in sediments (Ding et al., 2016; Chen et al., 2019). Under anaerobic conditions, iron (Fe^{3+}) in the surface sediment is reduced to ferrous (Fe^{2+}). This was accompanied by the reduction and dissolution of Fe-P in sediment, leading to a strong release of internal P (Fig. 3a). When ONBMM was added, the DO level of SWI rose sharply, and Fe was mainly present in the form of oxides (such as Fe oxide or hydroxide) near the SWI (Froelich et al., 1979). The strong adsorption capacity of iron oxides could prevent the desorption and release of active P in sediments (Nóbrega et al., 2014). In summary, the ONBMM changed the valence of iron by increasing DO levels in the vicinity of the SWI, and then inhibited the release of P from sediment. This supported the view that aerating SWI effectively inhibited the release of P in sediments (Yu et al., 2019).

Table 1
Release fluxes of TP, TN, NH_3-N from sediment in cores treated and untreated with ONBMM.

Sediment nutrient release flux ($mgm^{-2}d^{-1}$)	Treated with ONBMM			Untreated with ONBMM		
	A	B	ave	C	D	ave
TP	−0.72	−0.60	−0.66	5.58	3.39	4.49
TN	−55.74	−62.82	−59.28	−5.33	−23.25	−14.29
NH_3-N	4.86	6.07	5.46	23.72	19.56	21.64

3.4. Mechanism of ONBMM reducing nitrogen release in sediments

i. Effect of ONBMM on N concentration in overlying water and release flux

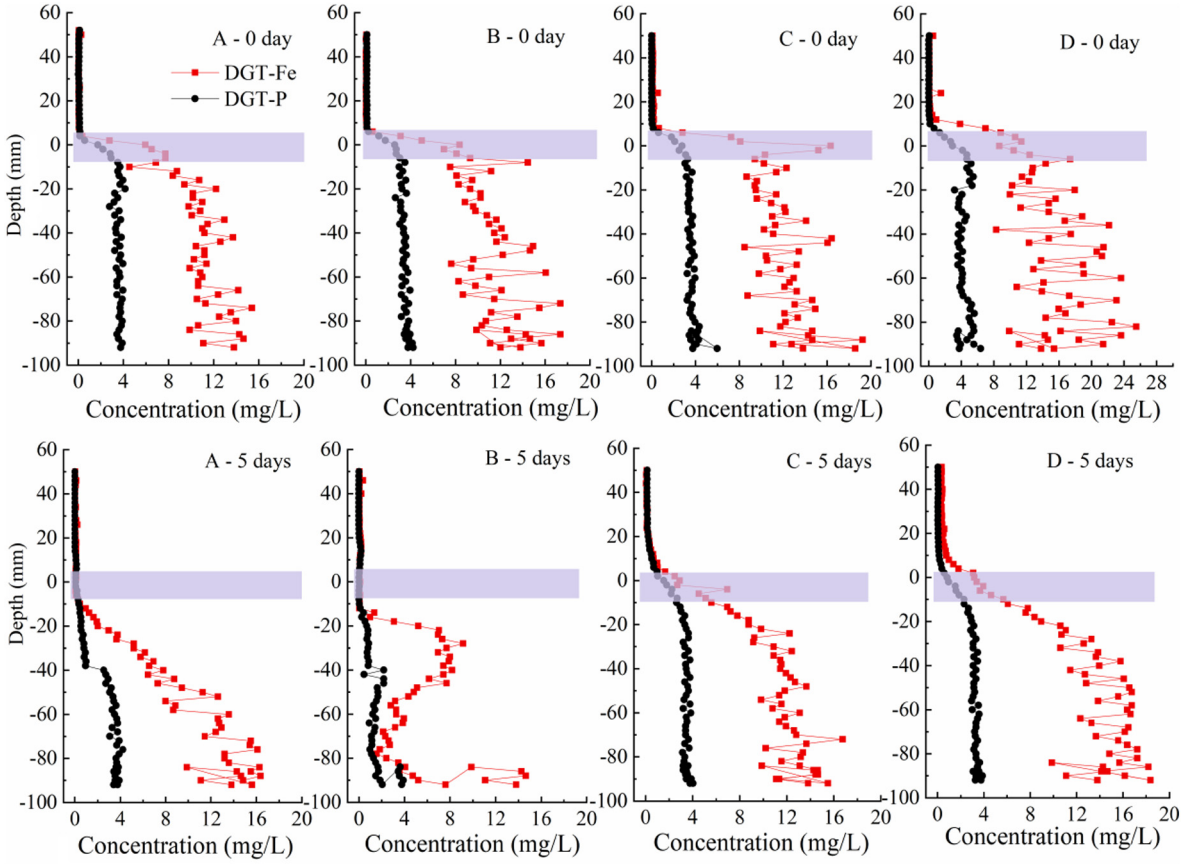

Fig. 4. Variation of DGT-P and DGT-Fe concentrations with depth at the sediment-water interface in cores treated (A, B) and untreated (C, D) with ONBMM.

In the group untreated with ONBMM, the average NH_3-N concentrations in the overlying water (Fig. 3b) continued to increase from 0.89 mgL^{-1} to 1.64 mgL^{-1}. The averageNH_3-N concentrations in the group treated with ONBMM in the overlying water were apparently lower compared to the group untreated with ONBMM. The average NH_3-N concentration in the overlying water showed a steady trend, with a removal rate reaching 51.1%. After adding ONBMM, the TN concentration first significantly decreased from 8.80 mgL^{-1} on Day 1 to 2.94 mgL^{-1} on Day 2, and then slowly increased to 6.96 mgL^{-1} on Day 25 (Fig. 3c). The TN concentration did not distinctly change over time in the group not treated with ONBMM. In this case, the increase of NH_3-N concentration in the overlying water indicates that nitrate N and/or nitrite N are transformed into ammonia N under simulated anaerobic conditions. If the release of reduced N in anoxic sediment is taken into account, the release of gaseous N to the air may occur in the overlying water through the biological reduction of oxidized N, so as to keep the TN concentration in the water stable. However, obviously, the average TN concentration in the group treated with ONBMM was lower compared to the group not treated with ONBMM. Compared to the group untreated with ONBMM, the TN removal rate of column cores in the group treated with ONBMM was 24.9%. Table 1 shows the release fluxes of TN and NH_3-N from sediment cores under different treatment conditions.

It was difficult to control the experimental levels of the oxygen load with the ONBMM treatment, this prevented the accurate control of DO levels near the SWI. Therefore, there were differences in the release flux between two parallel samples. Despite this, the comparative results of the monitoring data of NH_3-N, TN concentration and release flux (Table 1) in the overlying water still strongly suggest that ONBMM effectively inhibited the releases of TN, and NH_3-N from sediments. Obviously, the effect of microorganisms on the N cycle is very significant, which will elaborate in the next section.

ii. Changes in microbial community structure.

A total of 1,200,244 clean reads were produced from 12 samples after Ion S5 sequencing. Table 2 shows the number of OTUs, goods-coverage, and calculated Chao index, ACE index, Shannon index and Simpson index for the four sediment samples at a 97% similarity level. The goods-coverage of four samples all exceeded 97%, indicating that the sequencing depth of the sample essentially covered all species. The Chao, ACE, Shannon, and Simpson indices demonstrate that the untreated group and the treated group are similar in community richness and community diversity.

Fig. 5 shows the relative species abundance in the sediment samples at the phylum level (the top 10 species of the largest abundance). The bacterial community structure of sediment samples in the four groups showed a high diversity at the phylum classification level. *Proteobacteria*, *Chloroflexi*, *Bacterotides*, *Eyarchaeota* and *Planctomycetes* were the main phylum groups. There were no significant differences in the microbial species in the A, B, C and D groups; however, there were significant differences in the community structure (Fig. 5). The results of PCA analysis showed that the data for A, B, C and D showed differences and regularities (Fig. 6).

Table 2
OTUs data statistics, rDNA abundance, and diversity index for the four sediment samples at a 97% similarity level.

Samples	OTUS	Goods-coverage	ACE	Chao	Simpson	Shannon
A	5271	0.978	6324.789	6232.895	0.997	10.432
B	4953	0.983	5597.351	5520.828	0.989	9.914
C	5214	0.981	5915.005	5814.182	0.998	10.512
D	5240	0.982	5917.979	5847.670	0.997	10.503

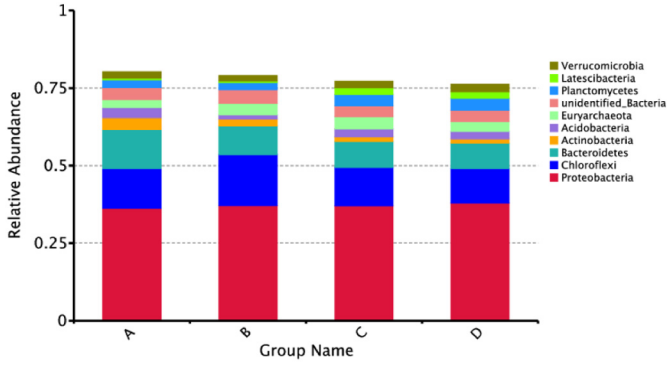

Fig. 5. Column graphs of the relative abundance of species at the phylum level (A and B denote the ONBMM treatment group; C and D denote the group untreated with ONBMM).

The proportion of relative abundance between specific bacterial species also reveals differences. The proportions of the relative abundance of *Cloroflexi* (14.62%), *Bacterooides* (10.92%) and *Actinobacteria* (6.96%) in the group with the added treatment were higher compared to untreated group. The relative abundance of *Proteobacteria* (37.51%), *Plantctomyces* (3.74%), *Euryarchaeota* (3.54%), *Acidobacteria* (2.51%), *Verrucomicrobia* (2.2%), *Latescibacteria* (2.16%) and *Actinobacteria* (1.40%) in the untreated group all exceeded those in the treated group. In the sediment microbial community, some bacteria were involved in nutrient recirculation in water, with the exception of the dominant flora. Fig. 7 shows the relative abundance of nitrobacteria, denitrifying bacteria, and ammonia oxidation bacteria detected in sediment samples. The microorganisms were identified at the phylum, class, order, family, and genus levels were identified using 16S rRNA amplicon sequencing. Eleven kinds of denitrified bacteria were involved, including nitrobacteria, denitrifying bacteria, and ammonia oxidation bacteria (Fig. 7). Hunter et al. (2006) showed that *Hyphomicrobaceae* can perform denitrification. *Plantctoceses* could convert nitrite and ammonia into nitrogen under anaerobic conditions, causing a distinctly loss in the fixed nitrogen in the hypoxia (Fuerst, 1995). Mergaert et al. (2003) isolated *Thermomonas* in the anaerobic denitrification reactor, which has better denitrification capacity. The presence of the above mentioned bacteria positively impacted nitrogen recirculation at the SWI.

Due to the presence of ammonia oxidation bacteria *Nitrosomonas* and *Candidatus_brocadia*, most of the N in sediments entered the

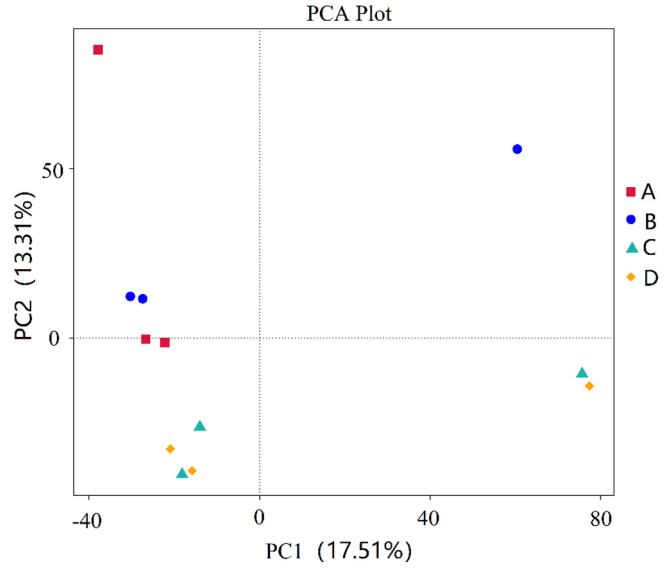

Fig. 6. Analysis diagram of PCA (A and B denote the ONBMM treatment group; C and D denote the group untreated with ONBMM).

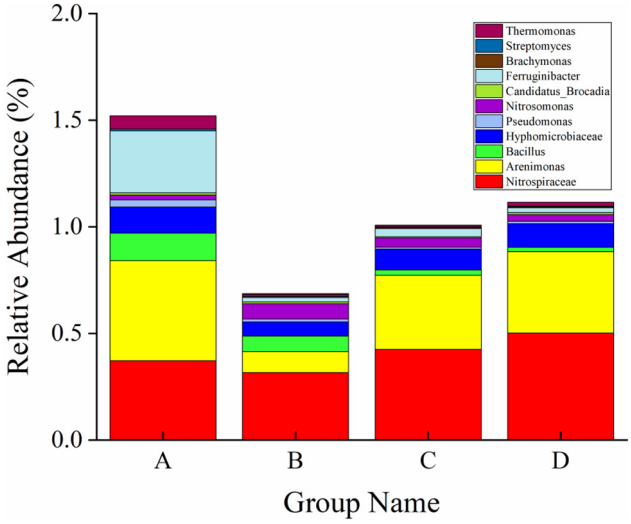

Fig. 7. Relative abundance of nitrobacteria, denitrifying bacteria, and ammonia oxidation bacteria (A and B denote the ONBMM treatment group; C and D denote the group untreated with ONBMM).

overlying water as exchangeable NH_4^+-N under anaerobic conditions. In the group treated with ONBMM, the DO concentration in the vicinity of the SWI obviously increased (Fig. 2A-B). This contributed to the nitrification of *Nitrosporaraceae*. This allowed NH_4^+-N to be converted into NO_3^--N (Rassamee et al., 2011). Thus, the NH_3-N concentration in the group treated with ONBMM was obviously lower compared to the group not treated with ONBMM (Fig. 3b). Also, anaerobic microorganisms had low requirement to N. The release of inorganic N as NH_3-N under anaerobic conditions exceeded the releases under aerobic conditions (Moore et al., 1992). Mccarthy et al. (2008) found that microorganisms could facilitate the reduction of NO_3^--N to NH_4^+-N under anaerobic conditions; that finding was consistent with this study's findings. The denitrification was then conducted under the action of denitrifying bacteria *Arimonas*, *Bacillus*, *Brachymonas*, *Exiguobacteria*, *Ferruginibacter*, *Pseudomonas*, *Stratomyces*, *Thermomonas*, and others. This converted NO_3^--N into N_2.The NO_3^--N concentration in the overlying water may decrease, and the intermediate product (NO_2^-N) may accumulate as a result. NO_2^- is both an oxidizer and a reducing agent; as such, it is itself instable. When the NO_3^--N concentration decreased, the NO_3^--N continuously transformed to become a low valence nitrogen substance under anoxic condition with a short supply (Schulthess et al., 1995), eventually reducing the released content. Although there was an exchange of NO_3^--N and NO_2^--N in the denitrifying bacteria at the SWI, the exchange had little effect on the concentrations in the overlying water under anaerobic conditions. In this study, the removal rate of NH_3-N in the overlying water was 51.1%. Compared with the control group, the decrease of NH_3-N concentration in the overlying water of the treated cores accounted for 44.8% of the decrease of TN concentration (Fig. 3b, c). It was assumed that NH_4^+-N removal dominated the removal of all forms of TN.

3.5. Factors influencing ONBMM development and its application in field engineering

The development and application of gaseous nano-technology currently remains in the exploration stage (Zhang et al., 2007). It is challenging to apply NBs to control lake water pollution (Pan et al., 2016), however, NB has distinct advantages in having low costs and rapid effects in conducting aeration at the lake SWI. Since the 21st century, scholars have studied the factors influencing the preparation and stability of NB. These have resulted in the following three insights. Firstly, low hydrophobic solid surfaces (contact angle <90°) require broad pretreatment to generate NB; in contrast, a highly hydrophobic surface

can be directly immersed into liquid to spontaneously form NB (Lou et al., 2002). Secondly, the cavity forming on the rough solid surface is strongly attracted to gas. Due to its small curvature, NB is more stable on a rough surface. Finally, when the base temperature increases (9 °C–30 °C), the number of NB increases significantly, peaking at approximately 40 °C. If the temperature continues to increase, the number of NB will gradually decrease (Yang et al., 2007).

NB has been recently applied to water treatment, pollutant removal and medical fields (Agarwal et al., 2011; Cai et al., 2015). However, transferring the application of NB to the SWI to achieve the effect of lake aeration faces some problems. Studies have not fully characterized the basic physicochemical properties of NB at the solid/liquid interface, the aeration mechanisms, and the risks to the ecological environment. In this study, the ONBMM has achieved some good effects in controlling the DO level and sediment N and P pollution at the SWI in lakes, however, some key problems still need to be solved in the field application of ONBMM technology. First, when the water body in the field is deep or strong hydrodynamic, NB may be lost in a short time. How to improve the gas carrying capacity of ONBMM? It is an important direction for future efforts. Meanwhile, the aging of ONBMM needs to be further quantified since the stabilization mechanism of NB is not clear (Pan et al., 2016; Ishida et al., 2000). Although it is reported that the stabilization time of NB can be >20 days at least (Shi et al., 2018), its continuance length is different in different lakes with varied seasonal oxygen deficiency duration, particularly in eutrophic lakes. Further research on the continuance length of ONBMM is needed. Moreover, in lakes with high sedimentation rates, ONBMM may be immediately buried under new sediments. That make it difficult to realize continuous oxygenation at the sediment surface using ONBMM. This limits the application of ONBMM technology in high deposition rate lakes. Therefore, problems such as the carrier gas flow, stability and time-effect, field addition, and environment risks of ONBMM should be considered when approaching practical engineering applications. Applying ONBMM technology to better control water pollution should be further studied and explored.

4. Conclusion

Simulation experiment shows that applying the ONBMM obviously improved DO concentrations in the 20 mm space near the SWI in the column cores, with a maximum DO concentration of 6.55 mgL^{-1}, indicating that ONBMM is a potentially effective technology for oxygenation at the SWI in lakes. Compared with traditional aeration technologies, the gas load and consumption of ONBMM are negligible; however, the aeration efficiency at the SWI is obviously high. This economic and efficient technology provides a new approach for aerating the SWI in lakes. Meanwhile, adding ONBMM remarkably inhibited the release of P from sediments, by increasing the DO level of surface sediments. In addition, adding ONBMM induced changes in the microbial community structure in surface sediments and strengthened the role of nitrobacteria, denitrifying bacteria, and ammonia oxidation bacteria. ONBMM changed the N circulation of SWI and simultaneously removed some of the ammonia N and TN in the overlying water. Given the good technical effect, simple operation, and low cost, ONBMM has a potential application prospect for aeration at the SWI and for the *in situ* control of internal pollution in eutrophic lakes and reservoirs.

CRediT authorship contribution statement

Jingfu Wang: Conceptualization, Methodology, Investigation, Writing - original draft, Writing - review & editing, Funding acquisition. **Jingan Chen:** Conceptualization, Methodology, Resources, Writing - review & editing. **Pingping Yu:** Investigation, Formal analysis. **Xiaohong Yang:** Formal analysis, Writing - review & editing. **Lijuan Zhang:** Investigation, Writing - review & editing. **Zhanli Geng:** Investigation. **Kangkang He:** Investigation.

Declaration of competing interest

The authors declare that they have no known competing financial interests or personal relationships that could have appeared to influence the work reported in this paper.

Acknowledgements

Authors would like to thank Assoc Professor Ståle Haaland and other anonymous reviewers for their constructive comments. This study was sponsored jointly by the Strategic Priority Research Program of Chinese Academy of Sciences (No. XDB40020300), the Chinese NSF Joint Fund Project (No. U1612441), the Chinese NSF project (Nos. 41773145, 41977296), the Guizhou Science and Technology Project of China ([2016]2802), the Youth Innovation Promotion Association CAS, and the CAS Interdisciplinary Innovation Team.

References

Agarwal, A., Ng, W.J., Liu, Y., 2011. Principle and applications of microbubble and nanobubble technology for water treatment. Chemosphere 84, 1175–1180.
Ashley, K.I., Mavinic, D.S., Hall, K.J., 2008. Oxygenation performance of a laboratory-scale Speece cone hypolimnetic aerator: preliminary assessment. Can. J. Civil Eng. 35, 663–675.
Beutel, M.W., Leonard, T.M., Dent, S.R., Moore, B.C., 2008. Effects of aerobic and anaerobic conditions on P, N, Fe, Mn, and hg accumulation in waters overlaying profundal sediments of an oligo-mesotrophic lake. Water Res. 42, 1953–1962.
Cai, W.B., Yang, H.L., Zhang, J., Yin, J.K., Yang, Y.L., Yuan, L.J., 2015. The optimized fabrication of nanobubbles as ultrasound contrast agents for tumor imaging. Sci. Rep. 5, 13725.
Chen, Q., Chen, J., Wang, J., Guo, J., Jin, Z., Yu, P., 2019. *In situ*, high-resolution evidence of phosphorus release from sediments controlled by the reductive dissolution of iron-bound phosphorus in a deep reservoir, southwestern China. Sci. Total Environ. 666, 39–45.
Ding, S.M., Wang, Y., Wang, D., Li, Y.Y., Gong, M., Zhang, C., 2016. *In situ*, high-resolution evidence for iron-coupled mobilization of phosphorus in sediments. Sci. Rep. 6, 24341.
Ducker, W.A., 2009. Contact angle and stability of interfacial nanobubbles. Langmuir 25, 8907–8910.
Fang, Z., Wang, L., Wang, X., Zhou, L., Wang, S., Zou, Z., 2018. Formation and stability of surface/bulk nanobubbles produced by decompression at lower gas concentration. J. Phys. Chem. C 122, 22418–22423.
Froelich, P.N., Klinkhammer, G.P., Bender, M.L., Luedtke, N.A., Heath, G.R., Cullen, D., 1979. Early oxidation of organic matter in pelagic sediments of the eastern equatorial Atlantic: suboxic diagenesis. Geochim. Cosmochim. Ac. 43, 1075–1090.
Fuerst, J.A., 1995. The planctomycetes: emerging models for microbial ecology, evolution and cell biology. Microbiology 141 (Pt7), 1493–1506.
Hunter, E.M., Mills, H.J., Kostka, J.E., 2006. Microbial community diversity associated with carbon and nitrogen cycling in permeable shelf sediments. Appl. Environ. Microb. 72, 5689–5701.
Ishida, N., Inoue, T., Miyahara, M., Higashitani, K., 2000. Nano-bubbles on a hydrophobic surface in water observed by tapping-mode atomic force microscopy. Langmuir 16, 6377–6380.
Lou, S., Gao, J., Xiao, X., Li, X., Li, G., Zhang, Y., 2002. Studies of nanobubbles produced at liquid/solid interfaces. Mater. Charact. 48, 211–214.
Mccarthy, M.J., Mcneal, K.S., Morse, J.W., Gardner, W.S., 2008. Bottom-water hypoxia effects on sediment–water Interface nitrogen transformations in a seasonally hypoxic, Shallow Bay (Corpus Christi Bay, TX, USA). Estuar. Coast. 31, 521–531.
McGinnis, D.F., Lorke, A., Wüest, A., Stöckli, A., Little, J.C., 2004. Interaction between a bubble plume and the near field in a stratified lake. Water Resour. Res. 40 (10). https://doi.org/10.1029/2004WR003038.
Mercier, P., Perret, J., 1949. Aeration station of Lake Bret. Monatsbull Schweiz Ver Gas Wasser-Fachm 29, 25.
Mergaert, J., Cnockaert, M.C., Swings, J., 2003. *Thermomonas fusca* sp. nov. and *Thermomonas brevis* sp. nov., two mesophilic species isolated from a denitrification reactor with poly (ε-caprolactone) plastic granules as fixed bed, and emended description of the genus *Thermomonas*. Int. J. Syst. Evol. Micr. 53, 1961–1966.
Moore, P.A., Reddy, K.R., Graetz, D.A., 1992. Nutrient transformations in sediments as influenced by oxygen supply. J. Environ. Qual. 21, 387–393.
Murphy, J., Riley, J.P., 1962. A modified single solution method for the determination of phosphate in natural waters. Anal. Chim. Acta 27, 31–36.
Nausch, M., Nausch, G., Lass, H.U., Mohrholz, V., Nagel, K., Siegel, H., 2009. Phosphorus input by upwelling in the eastern Gotland Basin (Baltic Sea) in summer and its effects on filamentous cyanobacteria. Estuar. Coast. Shelf S. 83, 434–442.
Nóbrega, G.N., Otero, X.L., Macías, F., Ferreira, T.O., 2014. Phosphorus geochemistry in a Brazilian semiarid mangrove soil affected by shrimp farm effluents. Environ. Monit. Assess. 186, 5749–5762.
Pan, G., He, G., Zhang, M., Zhou, Q., Tyliszczak, T., Tai, R., 2016. Nanobubbles at hydrophilic particle–water interfaces. Langmuir 32, 11133–11137.
Parker, J.L., Claesson, P.M., Attard, P., 1994. Bubbles, cavities, and the long-ranged attraction between hydrophobic surfaces. J. Phys. Chem. 98, 8468–8480.

Rassamee, V., Sattayatewa, C., Pagilla, K., Chandran, K., 2011. Effect of oxic and anoxic conditions on nitrous oxide emissions from nitrification and denitrification processes. Biotechnol. Bioeng. 108, 2036–2045.
Schulthess, R.V., Kühni, M., Gujer, W., 1995. Release of nitric and nitrous oxides from denitrifying activated sludge. Water Res. 29, 215–226.
Seddon, J.R., Kooij, E.S., Poelsema, B., Zandvliet, H.J., Lohse, D., 2011. Surface bubble nucleation stability. Phys.Rev.Lett. 106, 056101.
Serra, T., Vidal, J., Casamitjana, X., Soler, M., Colomer, J., 2007. The role of surface vertical mixing in phytoplankton distribution in a stratified reservoir. Limnol. Oceanogr. 52, 620–634.
Shi, W.Q., Pan, G., Chen, Q.W., Song, L.H., Zhu, L., Ji, X.N., 2018. Hypoxia remediation and methane emission manipulation using surface oxygen nanobubbles. Environ. Sci. Technol. 25 (15), 8712–8717.
Smith, V.H., 2003. Eutrophication of freshwater and coastal marine ecosystems a global problem. Environ. Sci. Pollut. R. 10, 126–139.
Smith, V.H., Schindler, D.W., 2009. Eutrophication science: where do we go from here? Trends Ecol. Evol. 24, 201–207.
Tamura, H., Goto, K., Yotsuyanagi, T., Nagayama, M., 1974. Spectrophotometric determination of iron(III) with 1, 10-phenanthroline in the presence of large amounts of iron(III). Talanta 21, 314–318.
Tyrrell, J.W.G., Attard, P., 2001. Images of nanobubbles on hydrophobic surfaces and their interactions. Phys. Rev. Lett. 87, 176104.
Ushikubo, F.Y., Furukawa, T., Nakagawa, R., Enari, M., Makino, Y., Kawagoe, Y., 2010. Evidence of the existence and the stability of nano-bubbles in water. Colloid. Surface A 361, 31–37.
Wang, J.F., Chen, J.A., Ding, S.M., Guo, J., Xu, Y., 2015. Effects of temperature on phosphorus release in sediments of Hongfeng Lake, SW China: an experimental study using diffusive gradients in thin-films technique. Environ. Earth Sci. 74, 5885–5894.
Wang, J.F., Chen, J.A., Ding, S.M., Guo, J., Christopher, D., Dai, Z.H., 2016. Effects of seasonal hypoxia on the release of phosphorus from sediments in deep-water ecosystem: a case study in Hongfeng reservoir, Southwest China. Environ. Pollut. 219, 858–865.
Wang, J.F., Chen, J.A., Guo, J., Dai, Z.H., 2017a. Speciation and transformation of sulfur in freshwater sediments: a case study in Southwest China. Water Air Soil Poll 228 (10), 392–403.
Wang, X., Zhao, B., Hu, J., Wang, S., Tai, R., Gao, X., 2017b. Interfacial gas nanobubbles or oil nanodroplets? Phys. Chem. Chem. Phys. 19, 1108–1114.
Yang, S., Dammer, S.M., Bremond, N., Zandvliet, H.J., Kooij, E.S., Lohse, D., 2007. Characterization of nanobubbles on hydrophobic surfaces in water. Langmuir 23, 7072–7077.
Yu, P.P., Wang, J.F., Chen, J.A., Guo, J., Yang, H., Chen, Q., 2019. Successful control of phosphorus release from sediments using oxygen nano-bubble-modified minerals. Sci. Total Environ. 663, 654–661.
Yue, F., Liu, C., Li, S., Zhao, Z., Liu, X., Ding, H., 2014. Analysis of $\delta^{15}N$ and $\delta^{18}O$ to identify nitrate sources and transformations in Songhua River, Northeast China. J. Hydrol. 519, 329–339.
Zhang, H., Lyu, T., Bi, L., Tempero, G., Hamilton, D.P., Pan, G., 2018. Combating hypoxia/anoxia at sediment-water interfaces: a preliminary study of oxygen nanobubble modified clay materials. Sci. Total Environ. 637–638, 550–560.
Zhang, X.H., Khan, A., Ducker, W.A., 2007. A nanoscale gas state. Phys. Rev. Lett. 98, 136101.
Zhang, X.H., Maeda, N., Hu, J., 2008. Thermodynamic stability of interfacial gaseous states. J. Phys. Chem. B 112, 13671–13675.